Supporting Information

Emergence of a C15 Laves Phase in Diblock Polymer/Homopolymer Blends

Andreas J. Mueller,[†] Aaron P. Lindsay,[†] Ashish Jayaraman,[†] Timothy P. Lodge,[†,‡] Mahesh K. Mahanthappa,[†,*] and Frank S. Bates[†,*]

[†]Department of Chemical Engineering and Materials Science, Minneapolis, Minnesota 55455, United States
[‡]Department of Chemistry, University of Minnesota, Minneapolis, Minnesota 55455, United States

*Corresponding authors: bates001@umn.edu (F.S.B.); maheshkm@umn.edu (M.K.M.)

Experimental Section

Materials: Solvents and reagents were used as received from Sigma-Aldrich Chemical Co. unless mentioned otherwise. Styrene was sequentially distilled under vacuum from $CaH_2(s)$, followed by double vacuum distillation from di-*n*-butyl magnesium. 1,3-butadiene was purified by two sequential, bulb-to-bulb transfers from *n*-butyllithium at –4 °C. Cyclohexane was sparged with argon and passed through successive columns of activated alumina and Q5 catalyst to remove air and water.

Sample Preparation: Poly(styrene-*block*-1,4-butadiene) (SB) diblocks were synthesized through well-established means,[1] which we briefly summarize. To a solution of *sec*-butyl lithium in cyclohexane at 40 °C under argon was added purified styrene which was allowed to react for 4 h. Following, purified 1,3-butadiene was added to the reactor and allowed to react overnight (12 h). The reaction was quenched with acidic methanol and precipitated twice from methanol under ambient conditions prior to drying *in vacuo* until excess solvent was removed. The synthesis of poly(1,4-butadiene) (B) followed an identical procedure, except for the addition of styrene. Molecular characteristics of all polymers discussed herein are presented in Table S1. ^{1}H NMR analyses of all B diblock segments and homopolymers reveal ≤ 10 mol% 1,2-polybutadiene content. Blends were prepared by solubilizing measured amounts of homopolymer and diblock, alongside a small (< 0.2 wt. %) amount of 2,6-di-*tert*-butylhydroxytoluene (BHT) in benzene followed by freeze drying. BHT acts as an antioxidant to delay polymer degradation and is known not to affect phase behavior at this concentration.[2]

^{1}H NMR Spectroscopy: Quantitative ^{1}H NMR spectra were acquired using a Bruker Avance 400 MHz spectrometer under ambient conditions in $CDCl_3$ employing a 30 s pulse repetition delay. Spectra were referenced to residual solvent peak of $CDCl_3$ (δ 7.26 ppm). Compositions of SB diblocks were calculated by the relative abundance of benzylic and olefinic protons characteristic of styrene or butadiene repeat units, respectively. Molecular weights of SB diblocks and B

homopolymers were quantitatively calculated relative to the six methyl protons of the *sec*-butyllithium initiator end group. Spectra for all polymers discussed in the main text are presented in Figure S1.

Size Exclusion Chromatography (SEC): The molar mass dispersity ($Đ = M_w/M_n$) of each polymer was determined through SEC using a Viscotek GPCMax VE 2001 system affixed with three Agilent Technologies PLGel Mixed-B columns (350 mm x 7.5 mm) and a Viscotek VE 3580 refractive index detector running with a BHT-stabilized tetrahydrofuran (THF) eluent at a flow rate of 1 mL/min, calibrated against polystyrene standards. Typical analyses employed polymer concentrations ranging 1–10 mg/mL. Additionally, SEC with multi-angle light scattering (SEC-MALS) was used to verify the M_n values determined by ^{1}H NMR. This system consisted of two Agilent Polypore columns followed by a Wyatt Dawn Heleos II light scattering detector. BHT-stabilized THF at a flow rate of 1 mL/min was once again used as eluent. Analytical data are provided in Table S1, with RI traces for all polymer samples are overlaid in Figure S2.

Small-angle X-ray Scattering (SAXS): SAXS samples were prepared by subjecting blends, initially in the form of freeze-dried powders, to extended thermal annealing at elevated temperatures. Polymer samples (~30 mg) were loaded into hermetically sealed aluminum TZero DSC pans (DSC Consumables, Austin, MN) under argon, prior to heating them on hotplates at the desired annealing temperatures in open air. All samples were initially subjected to a brief pre-annealing period at 200 °C for ≤ 30 min, in order to densify the freeze-dried powder prior to extended annealing at a lower temperature $T \leq 200$ °C. Sample thermal annealing was generally carried out at the University of Minnesota–Twin Cities, prior to quenching in liquid nitrogen (LN2) in order to rapidly vitrify the poly(styrene) matrix of the SB diblock microstructure and preserve their ordered morphologies for transport to the Advanced Photon Source (Argonne, IL) for synchrotron SAXS analyses.

Temperature-dependent synchrotron SAXS studies were carried out at Sector 5-ID-D of the Advanced Photon Source at Argonne National Laboratories, and samples were heated with a Linkam hot-stage (±1 °C temperature accuracy). 1D-SAXS intensity profiles were generated by azimuthally integrating 2D-SAXS patterns and plotting average intensity versus momentum transfer vector magnitude, $|q| = 4\pi\sin(\theta/2)/\lambda$, with scattering angle θ and X-ray wavelength λ = 0.7293 Å. The experimental sample-to-detector distance was calibration using an Au-coated Si grating with 7200 lines/mm. Scattering patterns were also collected at Sector 12-ID-B of the APS utilizing λ = 0.886 Å with sample-to-detector distance calibrated with silver behenate. In both cases 2D patterns were integrated using the software provided at each beamline. In cases where anomalous scattering events lead to high intensity spots ("hot spots") in the 2D pattern, patterns were integrated using Datasqueeze (http://www.physics.upenn.edu/~heiney/datasqueeze/index.html). Relative peak positions in the resulting powder patterns were then calculated using Igor Pro version 6.37 in order to make phase assignments.[3] Specifically, expected peak positions for cubic (BCC, C15), tetragonal (σ), and hexagonal (C14, HEXc) phases were calculated utilizing equations S1, S2, and S3, respectively.

$$q_{\text{cubic}} = 2\pi\left(\frac{h^2+k^2+l^2}{a^2}\right)^{1/2} \tag{S1}$$

$$q_{\text{tetragonal}} = 2\pi\left(\frac{h^2+k^2}{a^2}+\frac{l^2}{c^2}\right)^{1/2} \tag{S2}$$

$$q_{\text{hexagonal}} = 2\pi\left(\frac{4(h^2+k^2+kl)}{3a^2}+\frac{l^2}{c^2}\right)^{1/2} \tag{S3}$$

The above equations employ lattice parameters a and c and Miller indices h, k and l. Allowed planes of reflection (hkl) depend on the symmetry of lattice in question: $Im\bar{3}m$ (BCC), $Fd\bar{3}m$ (C15), $P6_3/mmc$ (C14), $P4_2/mnm$ (σ), $p6mm$ (HEXc).

Unit cell data were further reduced to average particle sizes for direct comparison of the swelling effects of the homopolymer between observed phases. This was done by taking the SAXS-based unit cell volume, dividing by the number of particles per unit cell, and extracting a radius from this particle volume as equations S4-S8 show:

$$R_{\mathrm{BCC}} = \left(\frac{3}{8\pi}\right)^{1/3} a \tag{S4}$$

$$R_{\sigma} = \left(\frac{a^2 c}{40\pi}\right)^{1/3} \tag{S5}$$

$$R_{\mathrm{C14}} = \left(\frac{a^2 c \sin\frac{\pi}{3}}{16\pi}\right)^{1/3} \tag{S6}$$

$$R_{\mathrm{C15}} = \left(\frac{1}{32\pi}\right)^{1/3} a \tag{S7}$$

$$R_{\mathrm{HEXc}} = \left(\frac{3a^2 \sin\frac{\pi}{3}}{4\pi}\right)^{1/2} \tag{S8}$$

Note that the radius for HEXc refers to cylinder radii. In all other cases it refers an average particle radius.

Electron Density Reconstruction

In order to generate a real-space electron density map of the C15 diffraction pattern in Figure 2 of the main text (α = 1.08 SB-18/B-6 blend with ϕ_{SB} = 0.85 at 200 °C) the original q-values were rescaled by a factor of 4 (a = 210.9 Å). This was done in order to reduce the computational resources required by the charge flipping algorithm. Next the *JANA2006*[4] software was used to perform a Le Bail refinement of the pattern in order to extract structure factor intensities for each

observed Bragg reflection, assuming *Fd3(-)m* symmetry, with results plotted in Figure S7. These structure factor intensities were included in the input file for the *SUPERFLIP* charge flipping algorithm[5] attached near the end of this document (p. 24-25). After 10,000 iterations the algorithm converged 70 times with an overall agreement factor of ≤ 9 producing an averaged electron density map which was visualized using VESTA.[6] Shown in Figures 2B and 2C of the main text is a 90 % isosurface of the resulting map.

Additional Tables & Figures:

Table S1: Molecular parameters of SB diblock and B homopolymers used for blend morphology studies.

Sample	M_n (kg/mol)[a] (^{1}H NMR/SEC)	f_B[b]	N_B[c]	N_S[c]	$Đ$[d]
SB-18	$33._3/33._0$	0.18_5	90	396	1.08
SB-13	$31._0/33._1$*	0.12_8	57	386	1.08
B-2	2.1/2.6	1.0	35	-	1.11
B-3	3.2/3.5	1.0	54	-	1.09
B-6	5.7/5.9	1.0	97	-	1.08

[a] Polymer M_n determined by ^{1}H NMR end group analysis and SEC-LS; "*" indicates SEC with RI detection versus poly(styrene) standards. [b] B segment volume fraction from ^{1}H NMR using the literature homopolymer melt density values $\rho_s = 0.996$ g/cm^3 and $\rho_b = 0.826$ g/cm^3 at 140 °C [7]. [c] Segment density-normalized degree of polymerization calculated with respect to a 118 Å^3 reference volume using the respective melt homopolymer densities. [d] Sample dispersity from refractive index SEC in THF.

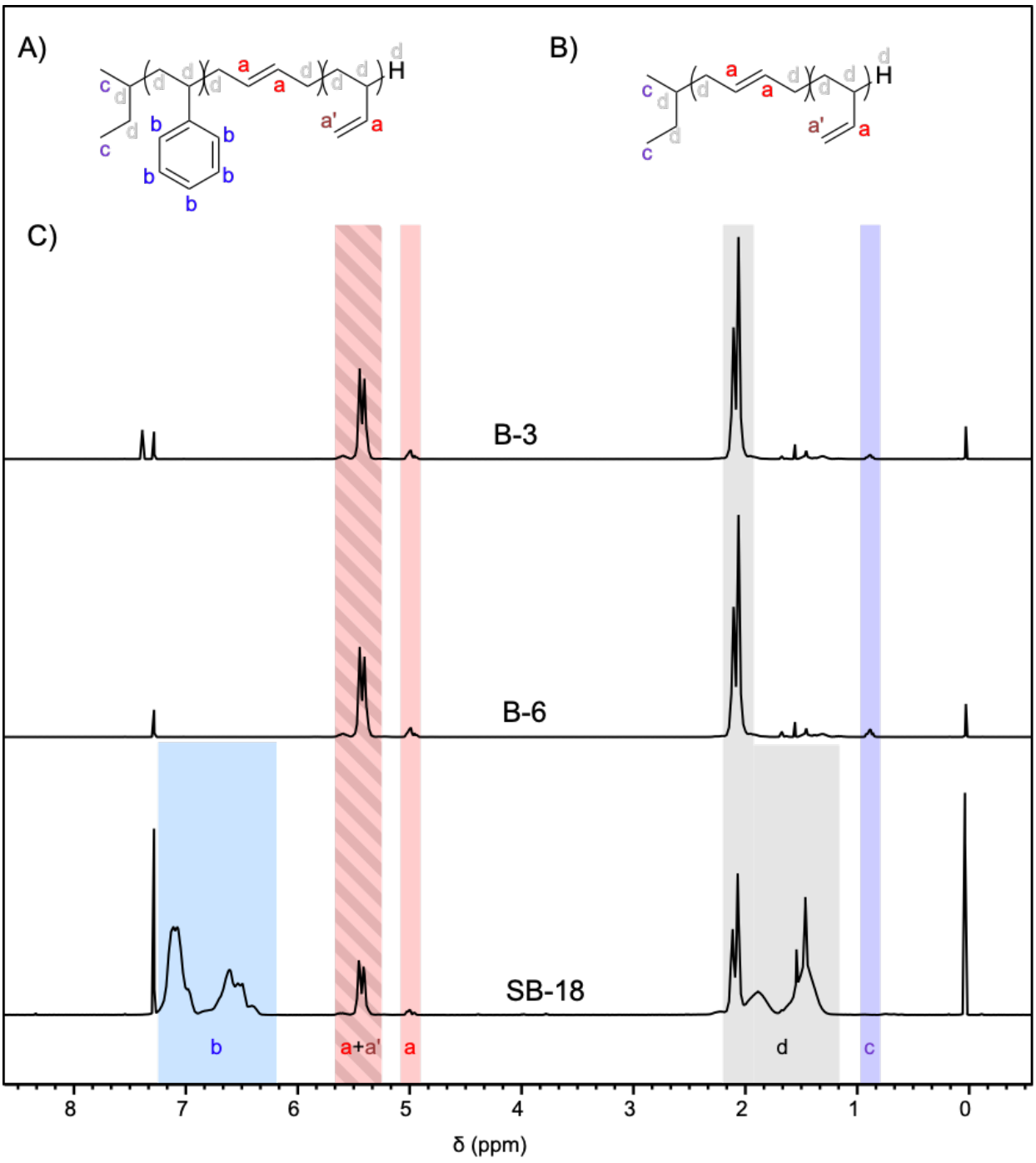

Figure S1: Chemical structures of (A) poly(styrene-*block*-1,4-butadiene) (SB-18) and (B) poly(1,4-butadiene), and (C) ^{1}H NMR spectra of poly(styrene-*block*-1,4-butadiene) (SB-18) and poly(1,4-butadiene) (B-3, B-6) homopolymers acquired in $CDCl_3$ at 22 °C. The relative integrated intensities of the vinylic peaks (*a, a'*), aromatic resonances (*b*), and $–CH_3$ resonances of the *sec*-butyl endgroup (*c*) were utilized for M_n determination; atom labels respectively correspond to Panels (A) and (B). Relative *b* and *a,a'* intensities were utilized in concert with literature density values to calculate the diblock volume fraction, f_B. Aliphatic peaks are labeled *d*.

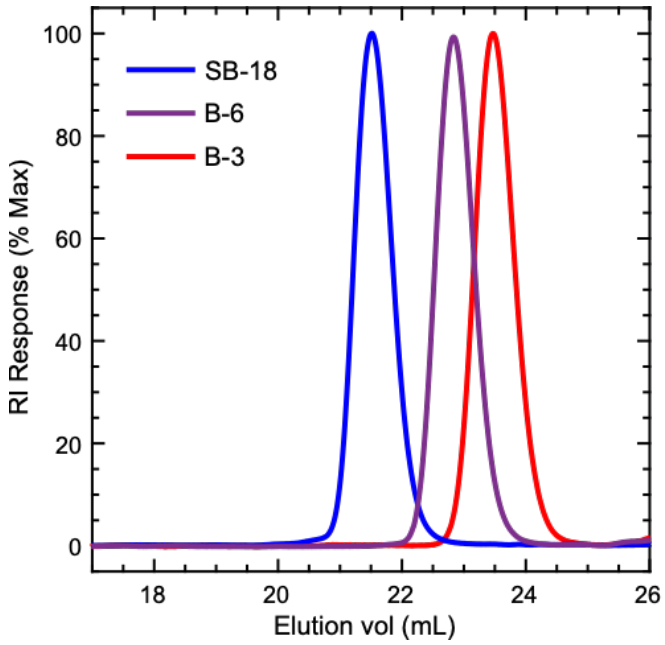

Figure S2: Overlay of SEC refractive index traces for SB-18, B-6 and B-3 discussed in the main text, which were acquired in THF eluent.

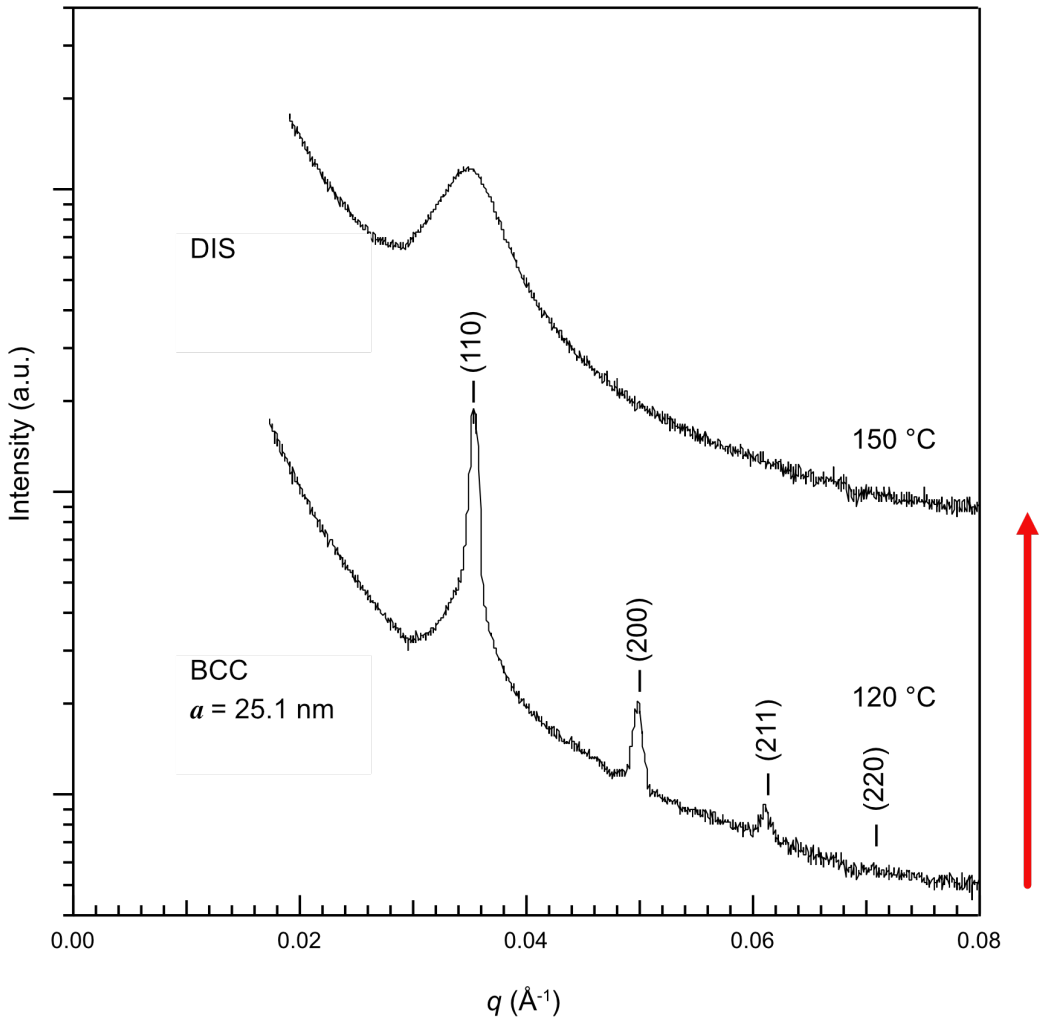

Figure S3: 1D temperature-dependent SAXS traces for neat SB-18, after annealing for 60 h at each temperature. The pattern obtained at 120 °C corresponds to a BCC sphere phase with lattice parameter a = 25.1 nm, whereas correlation-hole scattering of a disordered (DIS) diblock melt is observed when $T \geq 150$ °C.

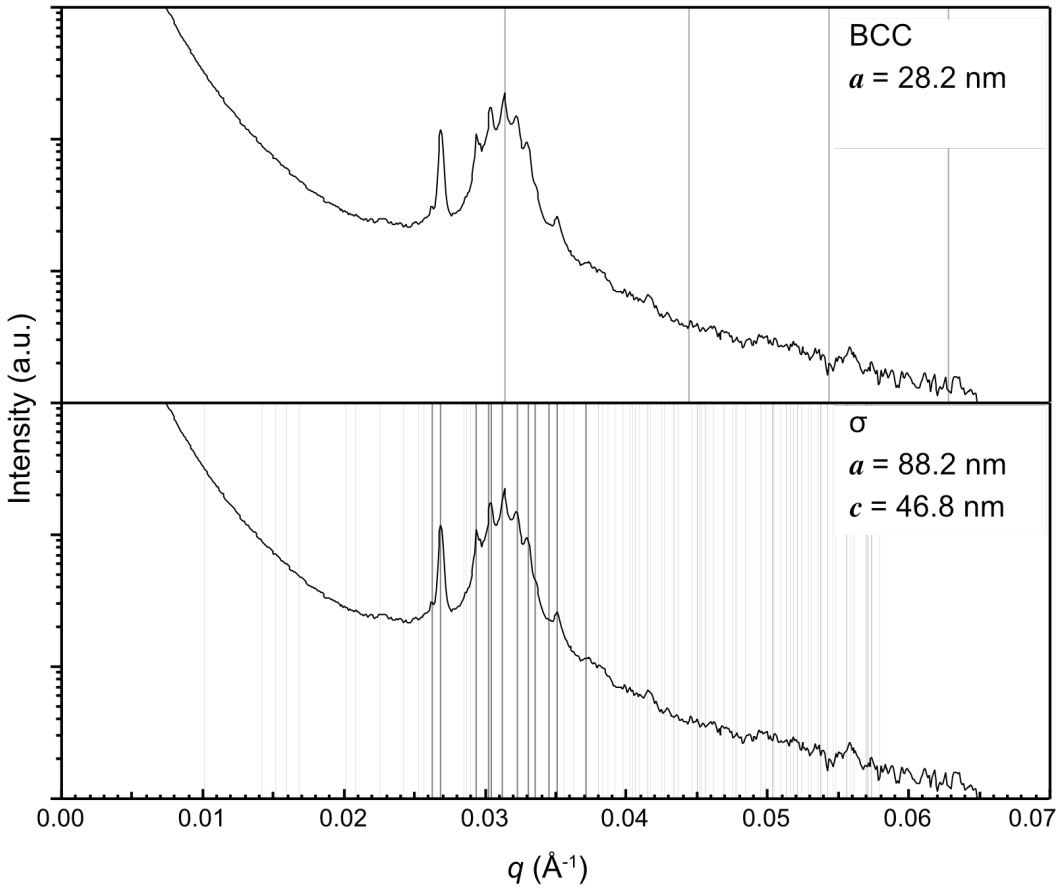

Figure S4: 1D-SAXS patterns of the α = 1.08 SB-18/B-6 blend with ϕ_{SB} = 0.97 annealed at 150 °C for 60 h shown with indexing lines to BCC (*top*) and σ (*bottom*) with lattice parameters indicated in each frame. No higher order BCC peaks were observed in the top frame suggesting the unusual intensity pattern does not arise from BCC/σ coexistence. Dark lines in the bottom frame indicate peaks listed in Table S2 as observed peaks for σ. The 2D-SAXS pattern associated with the bottom frame is given in Fig. S5(A).

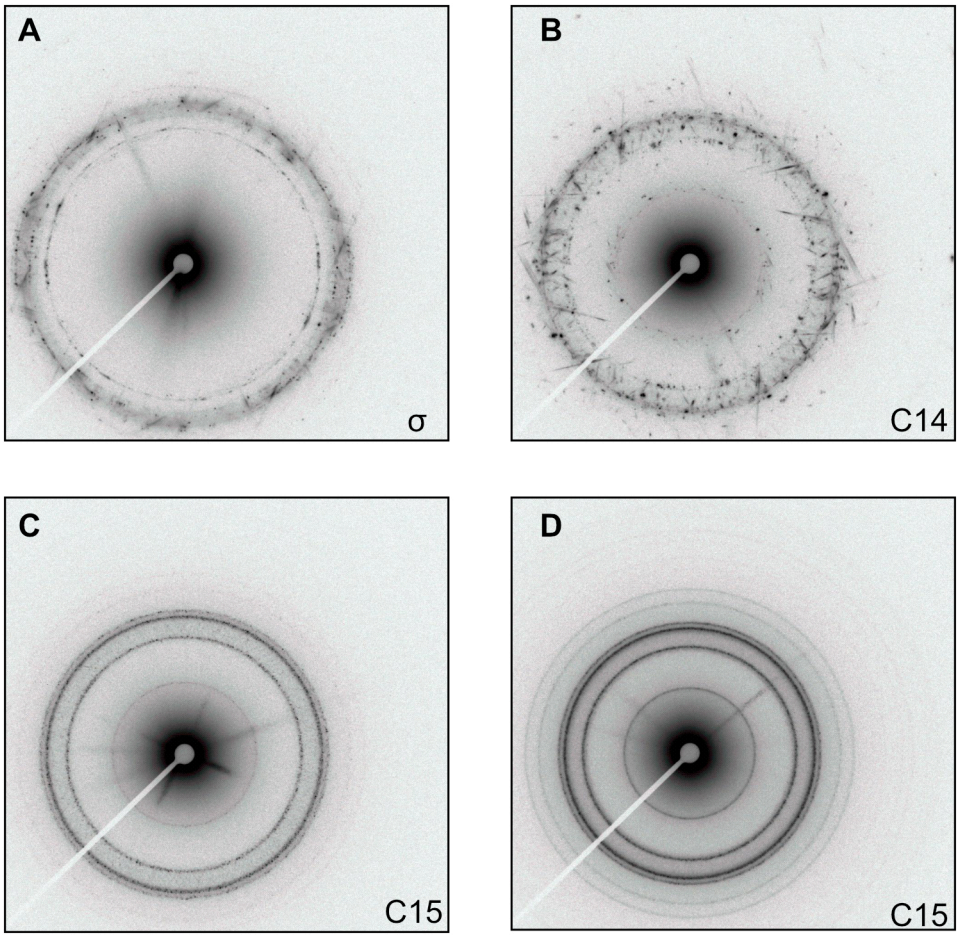

Figure S5: 2D-SAXS patterns of α = 1.08 SB-18/B-6 blends at different compositions after extended annealing for 24–60 h: (A) ϕ_{SB} = 0.97, T = 150 °C, (B) ϕ_{SB} = 0.93, T = 180 °C, (C), ϕ_{SB} = 0.89, T = 200 °C, and (D) ϕ_{SB} = 0.85, T = 200 °C, corresponding to the 1D traces shown in Figure 1A of the main text. The streaks in patterns (A) and (B) are most likely Bragg rods associated with stacking faults,[8] although multiple scattering in large grains may lead to a similar phenomenon.[9] The spotty textures observed in all patterns are indicative of large grain sizes with high degrees of long-range translational order.

Table S2: Calculated and observed peak positions of the FK σ phase ($P4_2/mnm$) in the $\alpha = 1.08$ SB-18/B-6 blend with $\phi_{SB} = 0.97$ annealed at 150 °C for 60 h. Calculations made with Eqn. S2 with $a = 88.2$ nm and $c = 46.8$ nm.

(h k l)	q_{calc} (Å^{-1})	q_{obs} (Å^{-1})	$\frac{\Delta q}{q_{calc}} \times 100$ %
(1 1 0)	0.0101	-	-
(2 0 0)	0.0142	-	-
(1 0 1)	0.0152	-	-
(2 1 0)	0.0159	-	-
(1 1 1)	0.0168	-	-
(2 2 0)	0.0201	-	-
(2 1 1)	0.0208	-	-
(3 1 0)	0.0225	-	-
(2 2 1)	0.0242	-	-
(3 0 1)	0.0252	-	-
(3 2 0)	0.0257	-	-
(3 1 1)	0.0262	0.0262	–0.081
(0 0 2)	0.0269	0.0269	–0.003
(4 0 0)	0.0285	-	-
(1 1 2)	0.0287	-	-
(3 2 1)	0.0290	-	-
(4 1 0)	0.0294	0.0294	–0.089
(3 3 0)	0.0302	0.0305	–0.834
(2 0 2)	0.0304	0.0304	0.128
(2 1 2)	0.0312	0.0314	–0.406
(4 1 1)	0.0323	0.0317	1.880
(3 3 1)	0.0331	0.0330	0.262
(2 2 2)	0.0336	0.0336	–0.071
(4 2 1)	0.0346	0.0345	0.174
(3 1 2)	0.0351	0.0351	–0.207
(5 1 0)	0.0363	-	-
(3 2 2)	0.0372	0.0373	–0.327
(4 3 1)	0.0381	-	-
(5 0 1)	0.0381	-	-
(5 1 1)	0.0387	-	-
(5 2 1)	0.0406	-	-

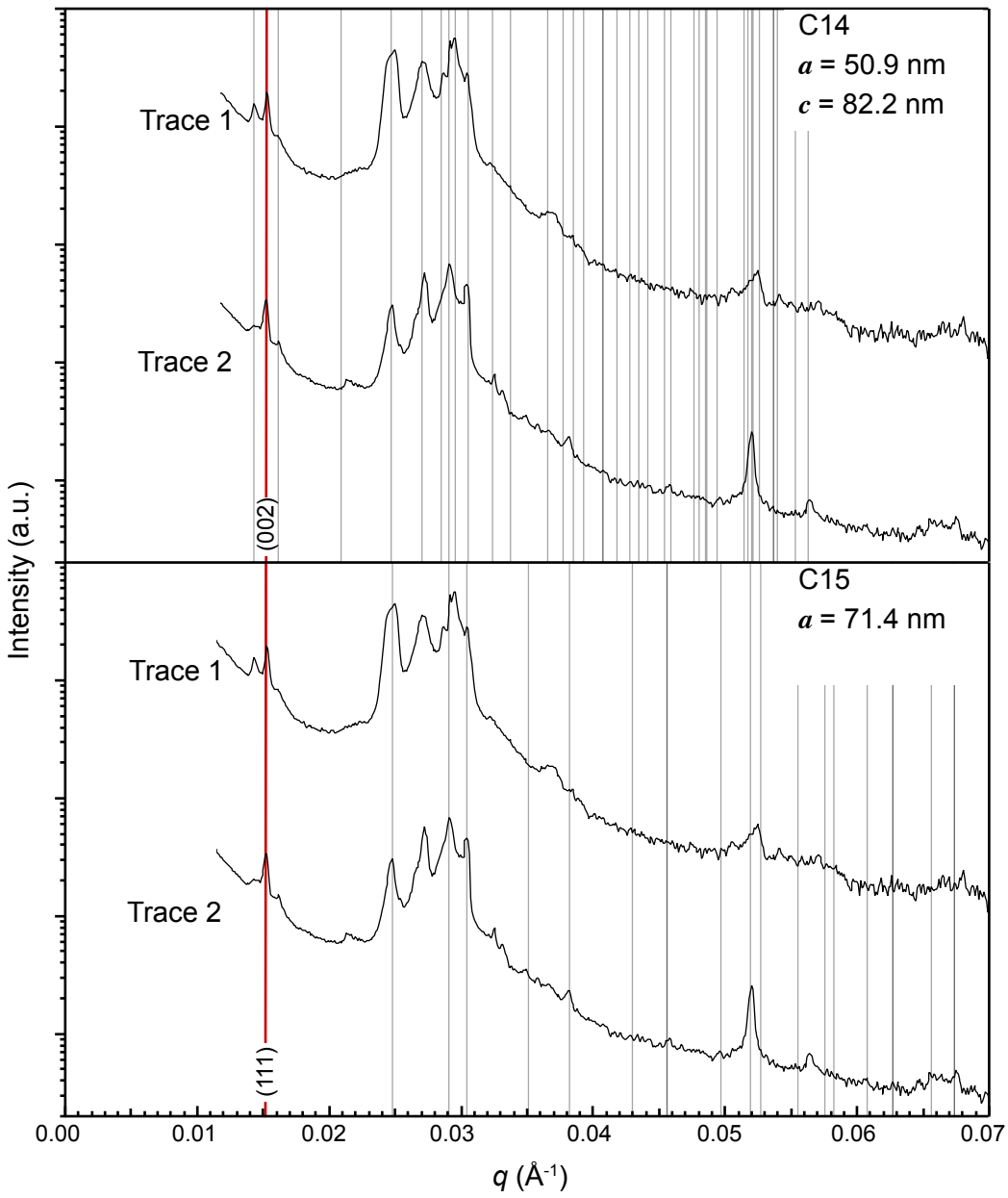

Figure S6: Indexed 1D-SAXS patterns for the $\alpha = 1.08$ SB-18/B-6 blend with $\phi_{SB} = 0.93$ annealed at 180 °C for 60 h. The different traces arise from SAXS analyses of the same sample at different positions. Residuals of peak positions in the top frame are presented in Table S3 and S4 for trace 1 and trace 2, respectively. The bottom frame shows pattern indexing to C15, which may coexist with the C14 phase in order to explain the unexpectedly high intensity C14 (002) near $q = 0.015$ Å^{-1}, which is expected to coincide with the (111) of the crystallographically-related C15 phase.

Table S3: Residuals of α = 1.08 SB-18/B-6 blend with ϕ_{SB} = 0.93 annealed at 180 °C for 60 h indexed to C14 ($P6_3/mmc$). Calculations made with Eqn. S3 with a = 50.9 nm and c = 82.2 nm. Indexing corresponds to Trace 1 in Figure S6.

(h k l)	q_{calc} (Å^{-1})	q_{obs} (Å^{-1})	$\frac{\Delta q}{q_{calc}} \times 100$ %
(1 0 0)	0.0143	0.0143	0.262
(0 0 2)	0.0153	0.0153	0.052
(1 0 1)	0.0162	0.0162	0.032
(1 0 2)	0.0209	-	-
(1 1 0)	0.0247	0.0245	–0.693
(1 0 3)	0.0270	0.0271	0.194
(2 0 0)	0.0285	0.0286	0.167
(1 1 2)	0.0291	0.0292	0.529
(2 0 1)	0.0295	0.0295	–0.203
(0 0 4)	0.0306	0.0305	–0.330
(2 0 2)	0.0324	-	-
(1 0 4)	0.0337	-	-
(2 0 3)	0.0366	-	-
(2 1 0)	0.0377	-	-

Table S4: Residuals of α = 1.08 SB-18/B-6 blend with ϕ_{SB} = 0.93 annealed at 180 °C for 60 h indexed to C14 ($P6_3/mmc$). Calculations made with Eqn. S3 with a = 50.9 nm and c = 82.2 nm. Indexing corresponds to Trace 2 in Figure S6.

(h k l)	q_{calc} (Å^{-1})	q_{obs} (Å^{-1})	$\frac{\Delta q}{q_{calc}} \times 100$ %
(1 0 0)	0.0143	0.0142	–0.369
(0 0 2)	0.0153	0.0152	–0.538
(1 0 1)	0.0162	0.0162	0.032
(1 0 2)	0.0209	0.0213	1.878
(1 1 0)	0.0247	0.024	0.376
(1 0 3)	0.0270	0.0272	0.852
(2 0 0)	0.0285	-	-
(1 1 2)	0.0291	0.0290	–0.086
(2 0 1)	0.0295	-	-
(0 0 4)	0.0306	0.0303	–0.925
(2 0 2)	0.0324	0.0324	0.226
(1 0 4)	0.0337	-	-
(2 0 3)	0.0366	-	-
(2 1 0)	0.0377	-	-

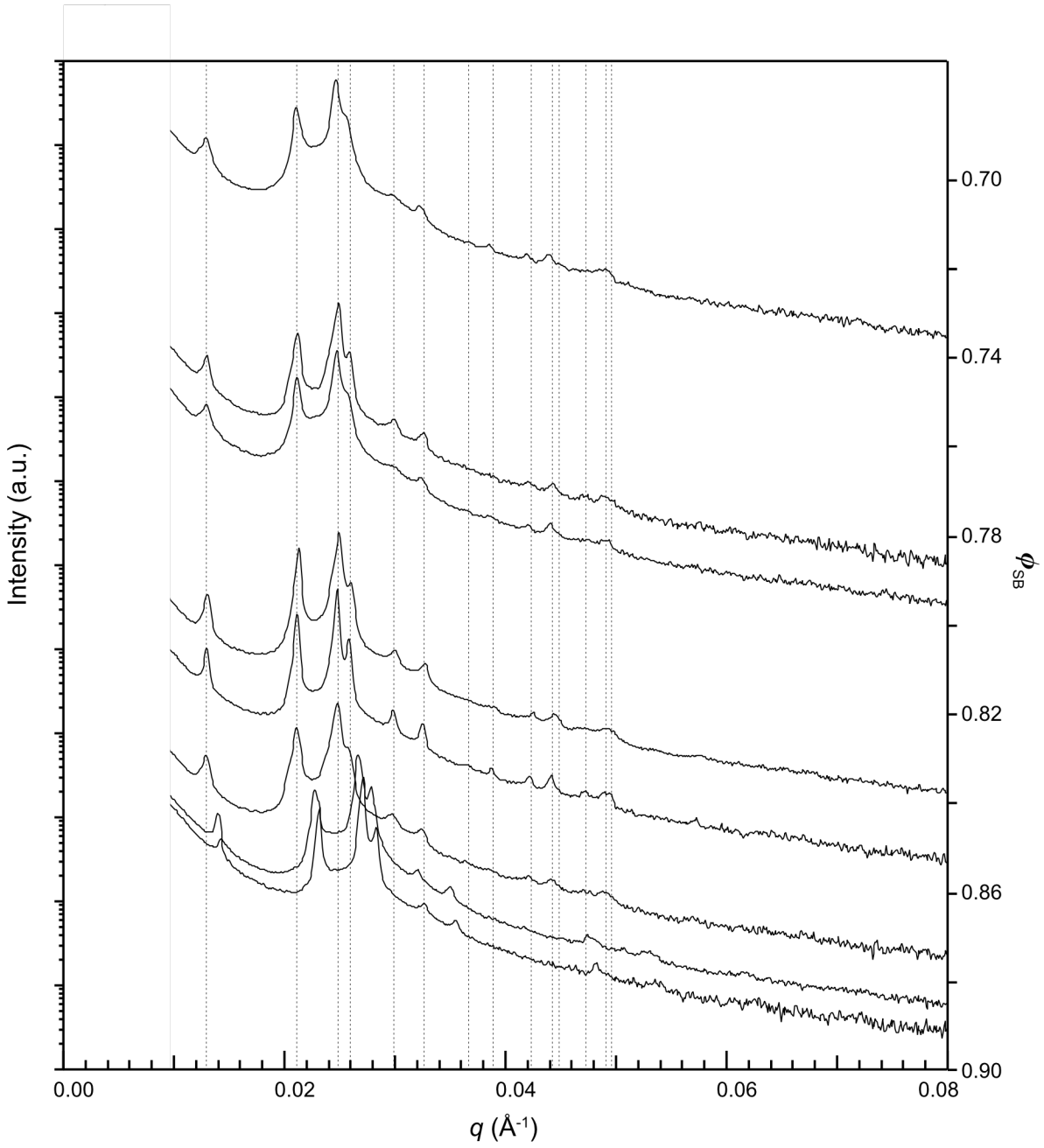

Figure S7: Evolution of 1-D SAXS for the C15 phase on increasing the homopolymer loading in the α = 1.08 SB-18/B-6 blends. All patterns were collected at 200 °C after 24 h of thermal annealing at the same temperature. The blend composition ϕ_{SB} is plotted along the right ordinate of the plot, such that blends near the top of the plot contain more B-6 homopolymer than those near the bottom. Indexing lines correspond to the saturated C15 structure (a = 84.2 nm). Note that the SAXS peaks in the bottom two traces are shifted to the right relative to this indexing scheme, indicating a smaller lattice spacing and incomplete swelling of the constituent particles.

Table S5: Residuals for C15 (F*d*3(-)*m*) identified in the $\alpha = 1.08$ SB-18/B-6 blend with $\phi_{SB} = 0.85$ annealed at 200 °C for 24 h. Calculations made with Eqn. S1 with $a = 84.2$ nm.

(h k l)	q_{calc} (Å^{-1})	q_{obs} (Å^{-1})	$\frac{\Delta q}{q_{calc}} \times 100$ %
(1 1 1)	0.0129	0.0130	0.31
(2 2 0)	0.0211	0.0211	0.17
(3 1 1)	0.0247	0.0248	0.31
(2 2 2)	0.0258	0.0259	0.21
(4 0 0)	0.0298	0.0298	0.03
(3 3 1)	0.0325	0.0325	0.08
(4 2 2)	0.0365	-	-
(3 3 3)	0.0387	0.0387	-0.06
(4 4 0)	0.0422	0.0421	-0.11
(5 3 1)	0.0441	0.0441	-0.01
(4 4 2)	0.0447	0.0446	-0.20
(6 2 0)	0.0472	0.0471	-0.18
(5 3 3)	0.0489	0.0487	-0.43
(6 2 2)	0.0495	0.0494	-0.11

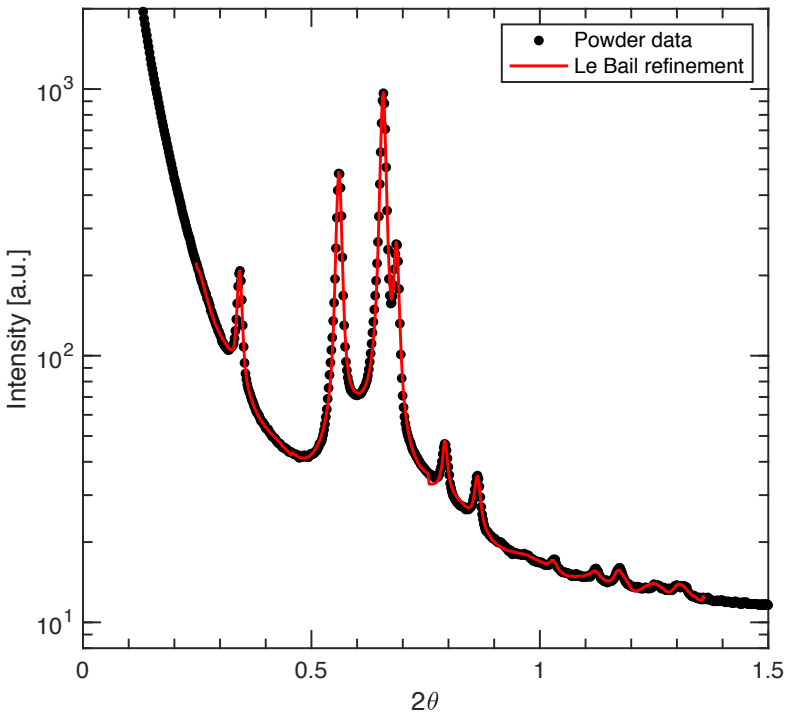

Figure S8: Le Bail Refinement of the C15 powder pattern in Figure 2 of the main text (α = 1.08 SB-18/B-6 blend with ϕ_{SB} = 0.85 annealed at 200 °C for 24 h). *JANA2006* was used for refinement, generating the structure factor intensities found in the *SUPERFLIP* input file on pg. 24-25 of this document.

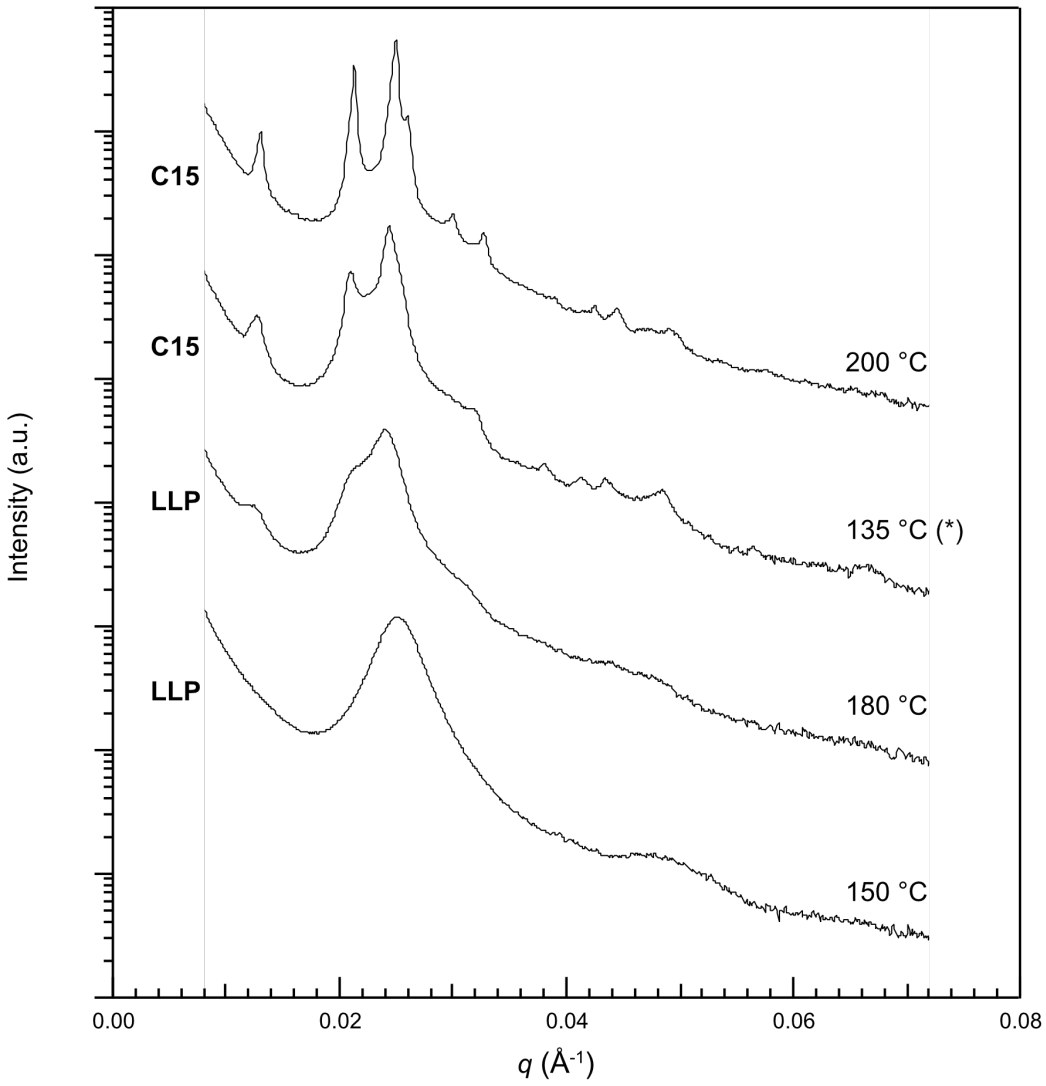

Figure S9: Annealing temperature dependence of C15 phase formation in a SB-18/B-6 blend with $\alpha = 1.08$ blend at $\phi_{SB} = 0.84$. The pattern obtained at 200 °C was taken after thermal annealing for 24 h at 200 °C. All SAXS samples were pre-annealed at 200 °C briefly (≤ 30 min) prior to extended annealing at the listed temperature for 60 h. The trace obtained at 135 °C (*) was pre-annealed at 200 °C for an extended period of 5 h. Enhanced long-range order is obtained particularly after annealing at high temperatures (200 °C), indicative of the substantial temperature-dependent kinetic barrier to ordered melt microphase separation.

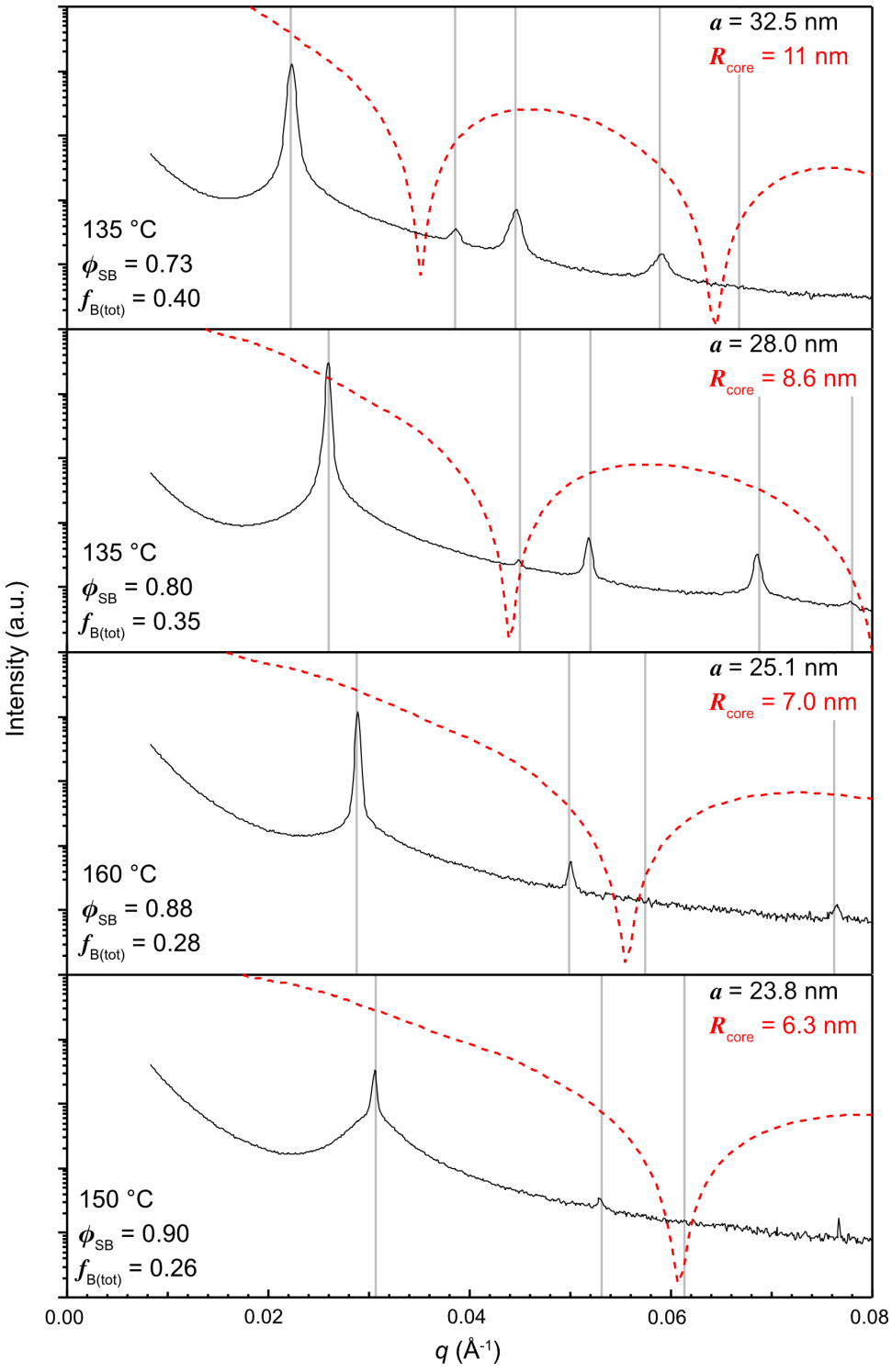

Figure S10: Indexed HEXc 1D-SAXS patterns from the SB-18/B-3 $\alpha = 0.60$ blend, given in the main text Figure 3b. Blend composition and annealing temperature are indicated in the bottom left of each frame. The red dotted lines correspond to cylindrical form factors for cylinders of arbitrary length, for which the cylinder radii and unit cell dimensions are indicated in grey and red, respectively, in each frame.

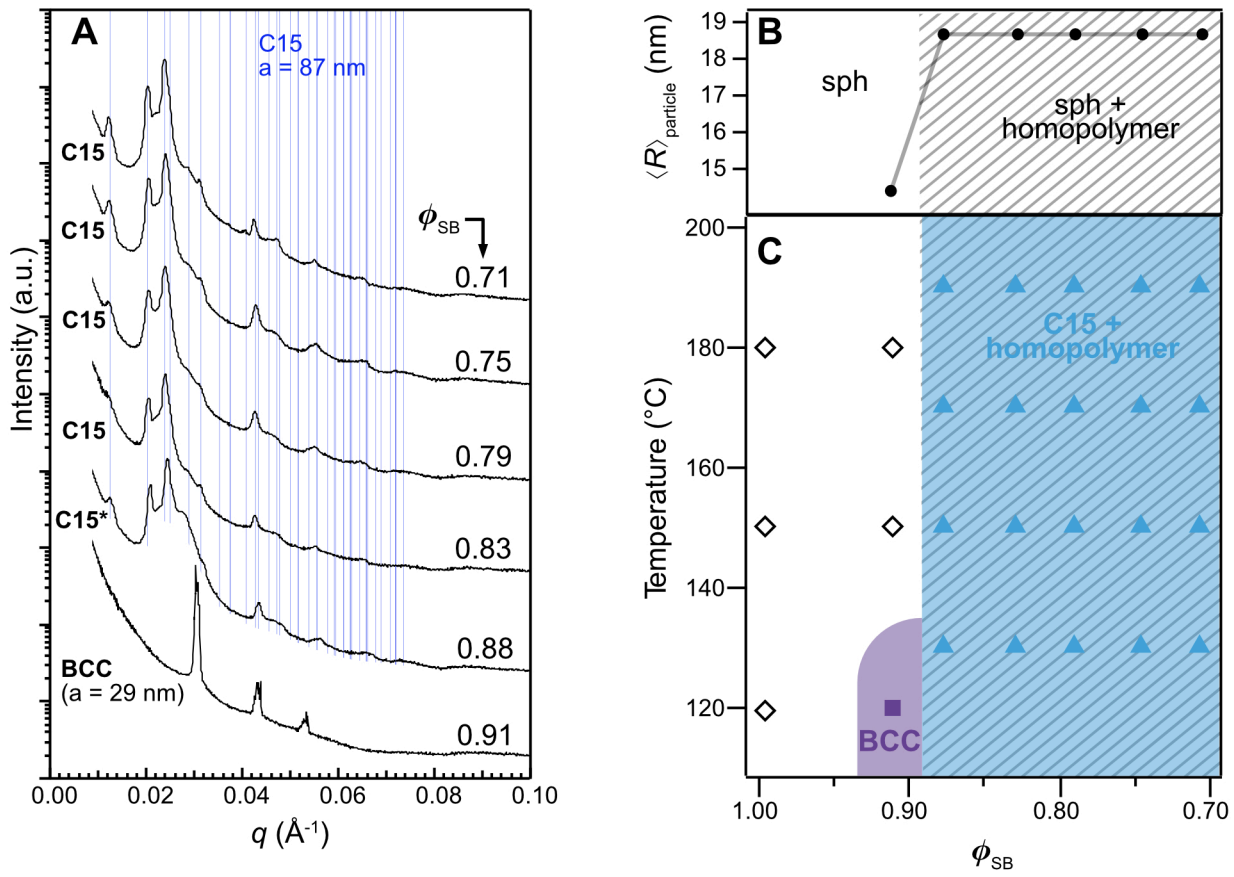

Figure S11: Phase behavior of blends of SB-13 and B-3 with $\alpha = 0.95$. (A) Representative 1D-SAXS traces taken at 150 °C, aside from the BCC pattern acquired at 120 °C. Blue indexing lines correspond to a C15 phase with $a = 87$ nm. (B) Plot of average particle size, based on a unit cell volume per particle, demonstrate evolution of particle radius with increasing homopolymer content. Saturation of particle size was taken as a signature of the onset of macrophase separation of homopolymer from the microphase separated diblock, and is indicated by the hatched regions in panels B and C. (C) Phase portrait of the blend.

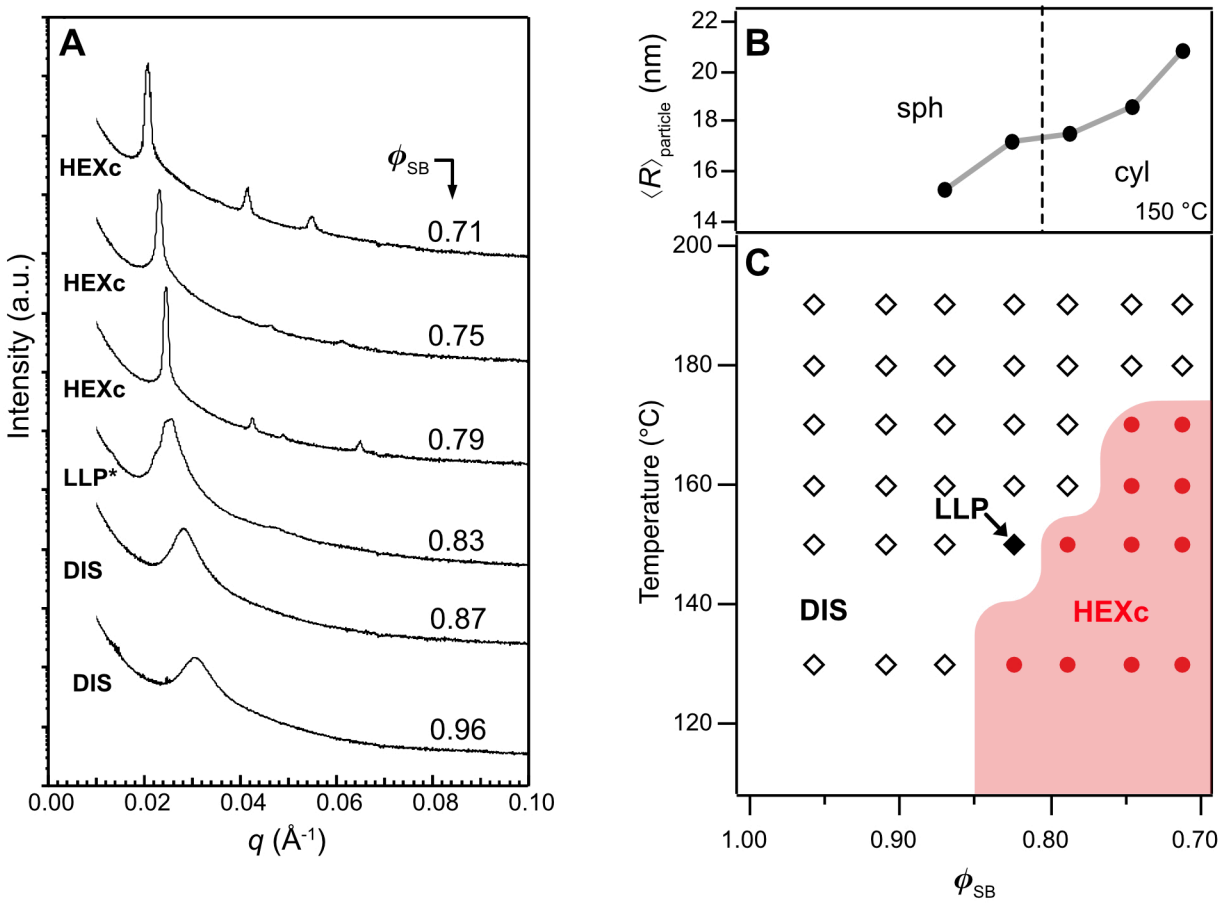

Figure S12: Phase behavior of SB-13/B-2 blends with α = 0.65. (A) Representative 1D-SAXS traces taken at 150 °C. The LLP* pattern displays a low-q shoulder, which in combination with its location near the sphere-cylinder transition in composition space implies the possibility of a narrow complex phase window in this blend. (B) Evolution of particle size, either average sphere (LLP) or circle (HEXc) radius; sphere radii for LLP patterns were estimated assuming BCC packing with the same primary SAXS peak position. (C) Phase portrait of the blend.

SUPERFLIP Input File for Charge Flipping

```
title C15_4xFV05
perform CF
outputfile "C15_4x10000.xplor"
outputformat xplor
dimension  3
cell   210.9170  210.9170  210.9170   90.00   90.00   90.00
spacegroup Fd-3m
centro yes
centers
  0.000000  0.000000  0.000000
  0.000000  0.500000  0.500000
  0.500000  0.000000  0.500000
  0.500000  0.500000  0.000000
endcenters
symmetry
      x1      x2      x3
 -x1+3/4 -x2+1/4  x3+1/2
 -x1+1/4  x2+1/2 -x3+3/4
  x1+1/2 -x2+3/4 -x3+1/4
      x3      x1      x2
  x3+1/2 -x1+3/4 -x2+1/4
 -x3+3/4 -x1+1/4  x2+1/2
 -x3+1/4  x1+1/2 -x2+3/4
      x2      x3      x1
 -x2+1/4  x3+1/2 -x1+3/4
  x2+1/2 -x3+3/4 -x1+1/4
 -x2+3/4 -x3+1/4  x1+1/2
  x2+3/4  x1+1/4 -x3+1/2
     -x2     -x1     -x3
  x2+1/4 -x1+1/2  x3+3/4
 -x2+1/2  x1+3/4  x3+1/4
  x1+3/4  x3+1/4 -x2+1/2
 -x1+1/2  x3+3/4  x2+1/4
     -x1     -x3     -x2
  x1+1/4 -x3+1/2  x2+3/4
  x3+3/4  x2+1/4 -x1+1/2
  x3+1/4 -x2+1/2  x1+3/4
 -x3+1/2  x2+3/4  x1+1/4
     -x3     -x2     -x1
     -x1     -x2     -x3
  x1+1/4  x2+3/4 -x3+1/2
  x1+3/4 -x2+1/2  x3+1/4
 -x1+1/2  x2+1/4  x3+3/4
     -x3     -x1     -x2
 -x3+1/2  x1+1/4  x2+3/4
  x3+1/4  x1+3/4 -x2+1/2
  x3+3/4 -x1+1/2  x2+1/4
     -x2     -x3     -x1
  x2+3/4 -x3+1/2  x1+1/4
 -x2+1/2  x3+1/4  x1+3/4
  x2+1/4  x3+3/4 -x1+1/2
 -x2+1/4 -x1+3/4  x3+1/2
      x2      x1      x3
 -x2+3/4  x1+1/2 -x3+1/4
  x2+1/2 -x1+1/4 -x3+3/4
 -x1+1/4 -x3+3/4  x2+1/2
  x1+1/2 -x3+1/4 -x2+3/4
      x1      x3      x2
 -x1+3/4  x3+1/2 -x2+1/4
 -x3+1/4 -x2+3/4  x1+1/2
 -x3+3/4  x2+1/2 -x1+1/4
  x3+1/2 -x2+1/4 -x1+3/4
      x3      x2      x1
endsymmetry
composition C397130 H873686
```

```
# Keywords for charge flipping
repeatmode 10000 sumgood
bestdensities 1 symmetry
polish yes
finevoxel 3.75 angstrom
maxcycles 4000
delta AUTO
weakratio 0.000
Biso   0.000
randomseed AUTO
searchsymmetry average
derivesymmetry no
# End of keywords for charge flipping

# EDMA-specific keywords
inputfile C15_4x10000.xplor
outputbase C15_4x10000
m40forjana yes
writem40 C15_4x10000.m40
maxima all
fullcell no
scale fractional
plimit    0.3000 sigma
numberofatoms composition
centerofcharge yes
chlimit    0.2500
chlimlist    0.0500 relative
# End of EDMA-specific keywords

electrons       0.0000
dataitemwidths 4 15 15
dataformat intensity fwhm
fbegin
   1   1   1       980.8108         0.0115
   2   0   2      6794.2622         0.0128
   1   1   3     10000.0000         0.0125
   2   2   2      6907.0313         0.0123
   0   0   4      1133.4384         0.0123
   3   1   3       268.0980         0.0146
   2   2   4         1.4988         0.0177
   1   1   5        42.6275         0.0194
   3   3   3        42.6275         0.0194
   4   0   4        88.6152         0.0219
   3   1   5        75.6165         0.0233
   4   2   4        75.7211         0.0238
   2   0   6         1.1937         0.0255
   3   3   5       167.1087         0.0267
   2   2   6       171.6875         0.0271
endf
```

References

(1) Ndoni, S.; Papadakis, C. M.; Bates, F. S.; Almdal, K. Laboratoryscale Setup for Anionic Polymerization under Inert Atmosphere Laboratory-Scale Setup for Anionic Polymerization under Inert Atmosphere. *Rev. Sci. Instrum.* **1995**, *66*, 1090–1095.

(2) Khandpurj, A. K.; Forster, S.; Bates, F. S.; Hamley, I. W.; Ryan, A. J. Diblock Copolymer Phase Diagram near the Order-Disorder Transition. *Macromolecules*. **1995**, *28*, 8796–8806.

(3) Schmitt, A. K.; Mahanthappa, M. K. Computer Code for Materials Scientists: Igor Pro Procedures for Analyzing Dynamic Light Scattering, Rheology, and Synchrotron X-ray Scattering Data.

(4) Petříček, V.; Michal, D.; Lukáš, P. Crystallographic Computing System JANA2006: General Features. *Z Kristallogr. Cryst. Mater.*. **2014**, 229, 345-352

(5) Palatinus, L.; Chapuis, G. SUPERFLIP - A Computer Program for the Solution of Crystal Structures by Charge Flipping in Arbitrary Dimensions. *J. Appl. Crystallogr.* **2007**, *40*, 786–790.

(6) Momma, K.; Izumi, F. VESTA 3 for Three-Dimensional Visualization of Crystal, Volumetric and Morphology Data. *J. Appl. Crystallogr.* **2011**, *44*, 1272–1276.

(7) Fetters, L. J.; Lohse, D. J.; Richter, D.; WItten, T. A.; Zirkel, A. Connection between Polymer Molecular Weight, Density, Chain Diomensions, and Melt Viscoelastic Properties. *Macromolecules*. **1994**, 4639–4647.

(8) Chen, L.; Lee, H. S.; Lee, S. Close-Packed Block Copolymer Micelles Induced by Temperature Quenching. *Proc. Natl. Acad. Sci. U. S. A.* **2018**, *115*, 7218–7223.

(9) Petukhov, A. V.; Dolbnya, I. P.; Aarts, D. G. A. L.; Vroege, G. J.; Lekkerkerker, H. N. W. Bragg Rods and Multiple X-Ray Scattering in Random-Stacking Colloidal Crystals. *Phys. Rev. Lett.* **2003**, *90*, 4.